TTP14-010

Goldstini and electroweak gauginos at the LHC

Ken-ichi Hikasa,[1] Tao Liu,[2] Lin Wang,[2] and Jin Min Yang[3]

[1]*Department of Physics, Tohoku University, Sendai 980-8578, Japan*

[2]*Institut für Theoretische Teilchenphysik,*
Karlsruhe Institute of Technology (KIT), D-76128 Karlsruhe, Germany

[3]*State Key Laboratory of Theoretical Physics,*
Institute of Theoretical Physics, Academia Sinica, Beijing 100190, China

Abstract

The multi-sector SUSY breaking predicts the existence of goldstini, which could couple more strongly to visible fields than ordinary gravitino. Then the lightest neutralino and chargino can decay into a goldstini plus a Z-boson, Higgs boson or W-boson. In this note we perform a Monte Carlo simulation for the direct productions of the lightest neutralino and chargino followed by the decays to goldstini. Considering scenarios with higgsino-like, bino-like or wino-like lightest neutralino, we find that the signal-to-background ratio at the high luminosity LHC is between 6 and 25% and the statistical significance can be above 5σ.

PACS numbers: 14.80.Da, 14.80.Ly, 12.60.Jv

I. INTRODUCTION

Supersymmetry (SUSY) remains the most popular theory for solving the hierarchy problem, albeit the recent discovery of a 125 GeV Higgs boson, which makes most low energy SUSY models suffer from fine-tuning to some extent [1]. From the viewpoint of model-building, the mechanism of SUSY breaking remains a puzzle. Usually, it is assumed that spontaneous breaking of SUSY occurs in some hidden sector and is mediated to visible fields by certain mechanism. Then a massless fermion named goldstino appears, which in the existence of local SUSY is absorbed into the longitudinal component of gravitino. If SUSY is broken in multiple sectors independently, each sector gives a goldstino η_i with SUSY breaking scale F_i. One linear combination of η_i is massless and eaten by the gravitino, while the orthogonal combination remains as a physical state and is named goldstini. The property and related phenomenology of goldstini have been investigated in the literature [2–16]. Comparing to the goldstino, the interactions of goldstini are not totally constrained by the supercurrent and thus some of its coulpings could be large enough to have intriguing phenomenology. In the framework of gauge mediated SUSY breaking (GMSB), goldstini can make final states softer and more structured at colliders [14]. In GMSB with more than two hidden sectors the multi-photon signature was discussed in [15] and the LHC detectability for the Higgs boson decay into a goldstini was examined in [16].

The non-observation of sparticles at the 7 TeV and 8 TeV runs of the LHC has set stringent bounds on colored sparticles. However, the electroweak sparticles are less constrained because of their small production rates, and can still have masses below 1 TeV. Theoretically, a light spectrum of electroweak sparticles is naturally predicted in some frameworks like anomaly mediation and non-minimal gauge mediations. So the study of electroweak sparticles, especially the light neutralinos and charginos, is rather important for testing SUSY at the LHC. At the LHC the neutralinos and charginos can be directly produced through the Drell-Yan process and vector boson fusion. In many conventional scenarios with R-parity, the lightest neutralino is stable and just leads to missing energy in the experiments. But in some low scale gauge mediation scenarios the lightest neutralino can decay into a photon plus a gravitino. In the scenario of SUSY breaking in two hidden sectors, the lightest neutralino can decay to a goldstini plus a Z-boson or Higgs boson. In this work we focus on such a two-sector SUSY breaking scenario to study the LHC detectability for the productions of lightest neutralino and chargino.

This work is organized as follows. In Section II we will make a brief review on the framework with goldstini and discuss its possible effect on the neutralino and chargino decays. Then in Section III we take an effective way to study the corresponding signal at the LHC. Finally, we give our conclusions in Section IV.

II. THEORETICAL REVIEW

Due to the non-renormalization theorem of superpotential, the spontaneous SUSY breaking is communicated to visible fields through the non-trivial Kähler potential K and gauge kinetic function f. After integrating the hidden sector fields and parameterizing their information in a non-linear way [18]

$$X_i = \frac{\eta_i^2}{2F_i} + \sqrt{2}\theta\eta_i + \theta^2 F_i, \tag{1}$$

the following representative term which contributes to the soft mass can be obtained

$$K = \Phi^\dagger\Phi \sum_i \frac{m_{\phi,i}^2}{F_i^2} X_i^\dagger X_i, \tag{2}$$

$$f_{ab} = \frac{1}{g_a^2}\delta_{ab}\left(1 + \sum_i \frac{2m_{a,i}}{F_i} X_i\right). \tag{3}$$

In the above equations, η_i is the so-called goldstino and $m_{\phi,a}$ are respectively the soft masses for the chiral fields and gauginos. The trilinear A terms and bilinear B_μ could also be constructed easily and we do not list them for simplicity. In the two-hidden-sector scenario with the definition $F = \sqrt{F_1^2 + F_2^2}$ and $\tan\theta = F_2/F_1$, the combination $G = \eta_1\cos\theta + \eta_2\sin\theta$ is eaten by the super-Higgs mechanism, while one goldstini $G' = -\eta_1\sin\theta + \eta_2\cos\theta$ is left. After substituting the expression of X_i and making some rotations, we get the interaction Lagrangian up to order $1/F_i$:

$$\mathcal{L}_G = \frac{m_\phi^2}{F} G\psi\phi^* - \frac{im_a}{\sqrt{2}F} G\sigma^{\mu\nu}\lambda^a F_{\mu\nu}^a + \frac{m_a}{F} G\lambda^a D^a, \tag{4}$$

$$\mathcal{L}_{G'} = \frac{\widetilde{m}_\phi^2}{F} G'\psi\phi^* - \frac{i\widetilde{m}_a}{\sqrt{2}F} G'\sigma^{\mu\nu}\lambda^a F_{\mu\nu}^a + \frac{\widetilde{m}_a}{F} G'\lambda^a D^a. \tag{5}$$

Here the parameters m and $\widetilde{m}$ are defined as

$$m_{\phi/a} = m_{\phi/a,1} + m_{\phi/a,2}, \quad \widetilde{m}_{\phi/a} = -m_{\phi/a,1}\tan\theta + m_{\phi/a,2}\cot\theta. \tag{6}$$

It is easily found that goldstini can have much stronger couplings than gravitino under the condition of a big hierarchy between F_1 and F_2. This will lead to different phenomenology comparing to the ordinary gravitino. As argued in [16], from the perspective of model building $\widetilde{m}_a$ can be rather small and safely neglected.

About the mass of goldstini, at tree level it comes from the intrisic property of SUGRA. Also it can get loop corrections, which are very model-dependent. In our analysis we assume that the goldstini mass is much smaller than the lightest neutralino and treat it massless.

Now we look at the effects of goldstini in concrete models. In the minimal supersymmetric standard model (MSSM), the Lagrangian for the neutralinos and charginos is given by

$$\mathcal{L} = -\frac{1}{2}Y_{ij}\chi_i\chi_j h^0 + G_{ij}\chi_i^\dagger\bar{\sigma}^\mu\chi_j Z_\mu + (I_{ij}\chi_i^\dagger\bar{\sigma}^\mu\chi_j^+ + L_{ij}\chi_j^{-\dagger}\bar{\sigma}^\mu\chi_i)W_\mu^- + h.c. \tag{7}$$

Here $\chi_{i,j}$ represent the four neutralinos in the gauge eigenbasis $\{\tilde{B}, \widetilde{W}^0, \tilde{H}_d^0, \tilde{H}_u^0\}$ and their mass matrix is given by

$$M_{\tilde{N}} = \begin{pmatrix} M_1 & 0 & -c_\beta s_W m_Z & s_\beta s_W m_Z \\ 0 & M_2 & c_\beta c_W m_Z & -s_\beta c_W m_Z \\ -c_\beta s_W m_Z & c_\beta c_W m_Z & 0 & -\mu \\ s_\beta s_W m_Z & -s_\beta c_W m_Z & -\mu & 0 \end{pmatrix}. \tag{8}$$

$\chi_{i,j}^\pm$ are charginos in the gauge eigenbasis $\{\widetilde{W}^+, \tilde{H}_u^+, \widetilde{W}^-, \tilde{H}_d^-\}$ and their mass matrix is given by

$$M_{\tilde{C}} = \begin{pmatrix} 0 & X^T \\ X & 0 \end{pmatrix}, \qquad X = \begin{pmatrix} M_2 & \sqrt{2}s_\beta m_W \\ \sqrt{2}c_\beta m_W & \mu \end{pmatrix}. \tag{9}$$

The couplings to the physical Higgs and gauge bosons are given by

$$Y = \frac{1}{2}\begin{pmatrix} 0 & 0 & g's_\alpha & g'c_\alpha \\ 0 & 0 & -gs_\alpha & -gc_\alpha \\ g's_\alpha & -gs_\alpha & 0 & 0 \\ g'c_\alpha & -gc_\alpha & 0 & 0 \end{pmatrix}, \quad G = \frac{g}{2c_W}\begin{pmatrix} 0 & 0 & 0 & 0 \\ 0 & 0 & 0 & 0 \\ 0 & 0 & 1 & 0 \\ 0 & 0 & 0 & -1 \end{pmatrix}, \tag{10}$$

$$I = g\begin{pmatrix} 0 & 0 & 0 & 0 \\ -1 & 0 & 0 & 0 \\ 0 & 0 & 0 & 0 \\ 0 & \frac{1}{\sqrt{2}} & 0 & 0 \end{pmatrix}, \quad L = g\begin{pmatrix} 0 & 0 & 0 & 0 \\ 0 & 0 & 1 & 0 \\ 0 & 0 & 0 & \frac{1}{\sqrt{2}} \\ 0 & 0 & 0 & 0 \end{pmatrix}. \tag{11}$$

Since the contribution in Eq. (5) is proportional to $\widetilde{m}_\phi^2/F$, there are two goldstini interaction terms which should be added to the above Lagrangian:

$$y_i G'\chi_i h^0 + \rho_i G'\chi_i \tag{12}$$

with the parameters Y_{ij} and ρ_i given by

$$y = \frac{1}{\sqrt{2}F}\begin{pmatrix} 0 \\ 0 \\ \widetilde{B}_\mu c_\alpha - \widetilde{m}_{H_d}^2 s_\alpha \\ \widetilde{m}_{H_u}^2 c_\alpha - \widetilde{B}_\mu s_\alpha \end{pmatrix}, \quad \rho = \frac{v}{\sqrt{2}F}\begin{pmatrix} 0 \\ 0 \\ \widetilde{m}_{H_d}^2 c_\beta + \widetilde{B}_\mu s_\beta \\ \widetilde{m}_{H_u}^2 s_\beta + \widetilde{B}_\mu c_\beta \end{pmatrix}. \tag{13}$$

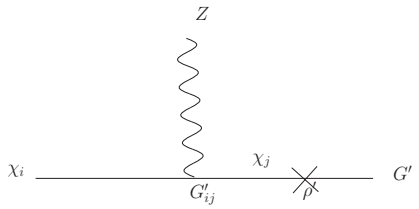

FIG. 1: A diagrammatic show of interactions between Z-boson and goldstini

In the above matrices, α and β are the mixing angles in the Higgs sector with $\tan\beta = \langle H_u^0\rangle/\langle H_d^0\rangle$. We used the notations $s_W = \sin\theta_W$, $c_W = \cos\theta_W$ (θ_W is the Weinberg angle) and $s_\beta = \sin\beta$, $c_\beta = \cos\beta$.

The linear terms induce a small mixing between neutralinos and goldstini, so we have to make a rotation to the mass eigenstate basis for neutralinos and then the small mass mixing can be treated perturbatively. For example, the vertex between Z-boson and goldstini G' appears after a mass insertion ρ', as shown in Fig. 1. The new matrices O'_i and O'_{ij} are defined as

$$O'_i = O_j N_{ji}, \quad O'_{ij} = O_{\ell m} N_{\ell i} N_{mj} \tag{14}$$

with $\chi \to N\chi$ to make mass matrix M' diagonal. Other interactions could be obtained in the same way, such as the interaction between chargino and goldstini. Now we can easily see that in this scenario the goldstini could not couple to photon or the transverse component of Z-boson and the two possible decay channels for the lightest neutralino are Z or h plus G'.

From the above analysis we can get the structure of the interactions for goldstini. However, there are many parameters involved, especially in the chargino and neutralino rotation matrices. So we only pick out some representative interactions to study the corresponding phenomenology.

To study the phenomenology, we employ the effective Lagrangian

$$\mathcal{L}_{\rm eff} = \frac{\widetilde{m}_\phi^2}{F}[g_{h\chi} h\chi^0 G' + g_{\chi Z}\bar{G}'\bar{\sigma}^\mu\chi^0 Z_\mu + g_{\chi W_1}\bar{G}'\bar{\sigma}^\mu\chi^+ W_\mu^- + g_{\chi W_2}\bar{G}'\bar{\sigma}^\mu\chi^- W_\mu^+ + h.c.]. \tag{15}$$

Here we list all possible couplings, some of which may be turned off in specific cases. The decay widths of the lightest neutralino and chargino to goldstini are given by

$$\Gamma(\chi^0 \to hG') = \frac{m_\chi}{16\pi}\frac{g_{h\chi}^2\widetilde{m}_\phi^4}{F^2}\left(1-\frac{m_h^2}{m_\chi^2}\right)^2, \tag{16}$$

$$\Gamma(\chi^0 \to ZG') = \frac{m_Z^2}{8\pi m_\chi}\frac{g_{\chi Z}^2\widetilde{m}_\phi^4}{F^2}\left(1-\frac{m_Z^2}{m_\chi^2}\right)\left[\frac{m_\chi^4}{2m_Z^4}+\frac{m_\chi^2}{2m_Z^2}-1\right], \tag{17}$$

$$\Gamma(\chi^\pm \to W^\pm G') = \frac{m_W^2}{16\pi m_\chi}\frac{(g_{\chi W_1}^2+g_{\chi W_2}^2)\widetilde{m}_\phi^4}{F^2}\left(1-\frac{m_W^2}{m_\chi^2}\right)\left[\frac{m_\chi^4}{2m_W^4}+\frac{m_\chi^2}{2m_W^2}-1\right]. \tag{18}$$

In our calculation we fix $\widetilde{m}_\phi/\sqrt{F} = 0.1$ and all the couplings g_X to be unity. Under these assumptions, the weak scale neutralino or chargino have the decay width at the order of $\sim 10^{-4}$ GeV and the decay length $\Gamma^{-1}\sqrt{(E^2 - m_\chi^2)/m_\chi^2} \sim 10^{-10}$ cm so they will decay inside the detector. Note that these parameters have no effects on the production rates of neutralino or chargino. As long as the neutralino and chargino only decay to goldstini, their signal rates are not sensitive to these parameters.

About the parameter space in the neutralino/chargino sector, following the analysis in [17], we classify it according to the relative values of $M_{1,2}$ and μ: (i) $|\mu| < M_1, M_2$; (ii) $M_2 < M_1, |\mu|$; (iii) $M_1 < M_2, |\mu|$. Each case corresponds to a different property of the lightest neutralino, called the lightest ordinary sparticle (LOSP). In the first case, the LOSP is higgsino-like, which can not only decay to Higgs, but also decay to Z-boson though a mass insertion of ρ. In the second and third cases the LOSP is respectively wino-like and bino-like, which only decays to a Higgs boson plus a goldstino through its mass mixing with the higgsino. For the lightest chargino, which is too light to decay into a neutralino plus an on-shell W-boson, it now can decay into a W-boson plus a goldstini. Note that in the second case the interaction vertex needs more than one insertion, so wino may mainly decay to gravitino. Since the decay to gravitino has the same collider signature, we assume the lightest chargino totally decay to goldstini.

III. PHENOMENOLOGICAL STUDY AT LHC

In this section we study the direct productions of the lightest neutralino and chargino followed by the decays to goldstini at the LHC. In our study we assume that other SUSY particles (like squarks, sleptons, heavy Higgs bosons and gluino) are heavy enough to be decoupled. The mass of the SM-like Higgs boson is fixed at $m_h = 125$ GeV. For the parameters M_1, M_2 and μ, they will be fixed with different values in three different cases listed in the preceding section. The sign of μ is assumed to be positive and $\tan\beta$ is fixed as 10 in the calculation. We use SOFTSUSY [19] to calculate the mass spectrum and the mixing matrices.

We use MadGraph5 [20] to perform Monte Carlo simulations for the signals and the SM backgrounds. The effective Lagrangian in Eq. (15) for the goldstini interaction is implemented in FeynRules [21] and passed the UFO model file [22] to MadGraph5. The signal and background samples are generated at parton level by MadGraph5 and then passed to Pythia [23] for parton shower and hadronization. The cross section of the signal is normalized to the Next-to-Leading-Order (NLO) by using Prospino2 [24]. The fast detector simulations are performed by using Delphes [25] with the ATLAS detector. For the clustering jets we

use the anti-k_t algorithm [26] with the radius parameter $\Delta R = 0.5$ in the FastJet package [27]. The sample analysis is performed with the package MadAnalysis5 [28].

A. Higgsino-like LOSP ($|\mu| < M_1, M_2$)

In this case the neutralino and chargino are produced mainly through the pairs $\chi_1^0\chi_1^\pm$, $\chi_2^0\chi_1^\pm$, $\chi_1^+\chi_1^-$, $\chi_1^0\chi_2^0$ (Note that if μ is much smaller than M_1 and M_2, then the higgsino-like χ_1^0, χ_2^0 and $\chi_1^\pm$ are nearly degenerate and such pair productions give no visible final states in the conventional MSSM with χ_1^0 being the LSP. In this case, to detect such productions at the LHC, an extra jet or photon is needed [29]). Their cross sections at the NLO can be found in [17]. Among these channels the production of $\chi_{1,2}^0\chi_1^\pm$ has the largest rate. In the two-hidden-sector SUSY breaking scenario, the neutralino decays to a Z-boson or Higgs plus a goldstini G', as discussed in Section II. Due to the large systematic uncertainty for the Higgs hadronic decay at the LHC, in this work we focus on the Z-boson mode and assume its branching ratio to be 0.5. With the leptonic decays of $Z/W^\pm$, the signal is

$$pp \to \chi_{1,2}^0\chi_1^\pm \to ZG'W^\pm G' \to \ell^+\ell^-\ell^\pm\nu G'G' \to 3\ell + \not{E}_T, \quad (\ell = e, \mu, \tau). \tag{19}$$

The relevant Feynman diagram is displayed in Fig. 2. Here the three leptons in the final state contain an oppositely charged lepton pair with same flavor. The tau lepton can be partially reconstructed from its hadronic decays. Note that the neutralino pair $\chi_1^0\chi_2^0$ can also contribute to the signal. We checked that its contribution is very small and can be neglected safely. The relevant mass parameters are fixed to $\mu = 200$ GeV, $M_1 = 1.0$ TeV and $M_2 = 1.5$ TeV as a benchmark scenario in the calculation.

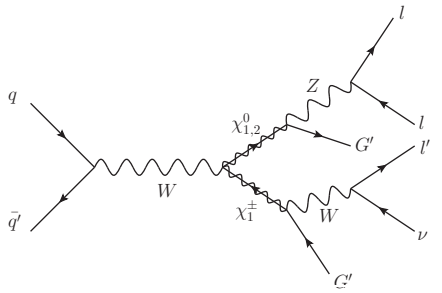

FIG. 2: Feynman diagram for the pair production of $\chi_{1,2}^0\chi_1^\pm$ followed by the subsequent decays into goldstini.

For the $3\ell + \not{E}_T$ final state, the dominant irreducible SM background is the WZ diboson production. We also consider other SM backgrounds including the top quark pair production, the diboson production of ZZ, the Z-boson production in association with jets. The top pair

production with di-leptonic decays may fake the signal since the b-jets and light jets may be misidentified as charged leptons. The contribution from this process can be suppressed by applying b-jets and light jets veto. For the background process ZZ with both Z bosons decaying to leptons, it can mimic our signal when one of the leptons is missing in the detector. In the case of $Z+j$ background, it may mimic our signal since a light jet may fake to charged lepton. These processes could be suppressed by requiring a large $\not{E}_T$. We do not consider the multi-lepton ($n \geq 3$) final state from the production of three gauge bosons due to its small cross section compared with other backgrounds.

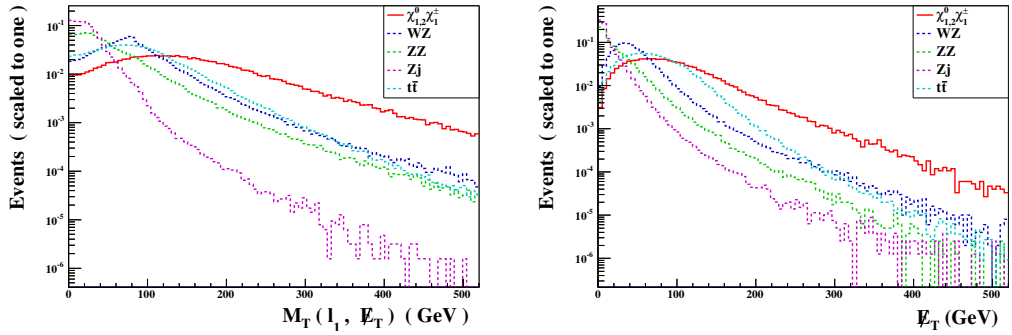

FIG. 3: The normalized M_T and $\not{E}_T$ distributions for the signal $pp \to \chi^0_{1,2}\chi^\pm_1 \to ZG'W^\pm G' \to \ell^+\ell^-\ell^\pm\nu G'G' \to 3\ell + \not{E}_T$ and background processes at the LHC with $\sqrt{s} = 14$ TeV. For the signal we fixed the relevant mass parameters as $\mu = 200$ GeV, $M_1 = 1.0$ TeV, $M_2 = 1.5$ TeV.

To efficiently cut the SM backgrounds, we in Fig. 3 plot some kinematic distributions for the signal and the backgrounds at the LHC with $\sqrt{s} = 14$ TeV. In the left frame of Fig. 3, we give the normalized transverse mass $M_T(\ell_1, \not{E}_T)$ distribution, where the definition of this variable is

$$M_T = \sqrt{2p_T^\ell \not{E}_T[1 - \cos\Delta\phi_{\ell,\not{E}_T}]}, \tag{20}$$

with $\Delta\phi_{\ell,\not{E}_T}$ being the azimuthal angle difference between the lepton and the missing energy. Here we use the lepton with the largest transverse momentum for constructing M_T. The right frame in Fig. 3 shows the normalized $\not{E}_T$ distribution. It is easy to see that a lower cut of about 120 GeV for M_T and 100 GeV for $\not{E}_T$ can improve the statistical significance of the signal. Based on these distributions, we apply the following event selection:

- Basic selection: three leptons with $p_T^{\ell_1,\ell_2,\ell_3} > 60, 40, 20$ GeV, $|\eta| < 2.5$. We use the following isolation criterion for electrons and muons: the transverse momentum sum of all charged particles with $p_T^{\rm min} > 0.5$ GeV that lie within a cone $R = 0.5$ around electron or muon should be less than 10% of transverse momentum of central electron or muon. Note that we assume the τ-tagging efficiency to be 40% and also include the mis-tags of QCD jets in Delphes.

- $M_T(\ell_1, \not{E}_T) > 120$ GeV.
- $\not{E}_T > 100$ GeV.
- The invariant mass of the oppositely charged lepton pair with same flavor must be within $|m_{\ell\ell} - m_Z| < 20$ GeV.
- Veto on tagged b-jets with $p_T > 20$ GeV and $|\eta| < 2.5$. We use the b-jet tagging and c-jet mis-tagging efficiency parametrization in [30]. Delphes also includes misidentification rate for light jets.
- Veto events with $p_T(j) > 60$ GeV and $|\eta| < 5.0$.

In Table I we present the numbers of signal and background events for the LHC with $\sqrt{s} = 14$ TeV and 100 fb^{-1} of integrated luminosity. We have normalized the cross section of the WZ production to NLO [31] and $t\bar{t}$ production to next-to-next-to-leading order (NNLO) [32]. From this table we can see that the signal is overwhelmed by the backgrounds after basic selection. As we excepted, the cut on the transverse mass M_T can suppress all the background processes significantly, especially for the electroweak processes. They are further reduced by requiring large missing transverse energy. Then the dominant irreducible SM background WZ is suppressed by about one order. The large background Zj has been completely removed. The other important background $t\bar{t}$ is also reduced by about a factor of seven. But the signal is decreased only a half. Though the invariant mass of charged lepton pair cut $|m_{\ell\ell} - m_Z| < 20$ GeV reduces both the signal and backgrounds, it improves the statistical significance of the signal efficiently. The final two cuts vetoing on b-jets and light jets are of crucial importance to further suppress the $t\bar{t}$ background. Note that the veto on the light jet also has a small effect on the signal due to the tau jet in the signal. After all cuts, the signal-to-background ratio is 6.3%.

In Table II we show the number of signal events and its significance before and after cuts for different luminosities at the 14 TeV LHC. Although the signal is reduced by applying cuts, its statistical significance is increased efficiently. With anintegrated luminosity of 1000–1500 fb^{-1}, the sensitivity can reach 5σ.

B. Wino-like LOSP ($M_2 < M_1, |\mu|$)

In this case, among the direct productions of neutralinos and charginos at the LHC, the pair production of $\chi_1^0\ \chi_1^\pm$ is dominant and we consider this process in our analysis. As discussed before, the LOSP χ_1^0 can only decay to a Higgs boson and a goldstini G' in this

TABLE I: The numbers of events for signal $pp \to \chi^0_{1,2}\chi^\pm_1 \to ZG'W^\pm G' \to \ell^+\ell^-\ell^\pm\nu G'G' \to 3\ell + \not{E}_T$ and backgrounds at the LHC with $\sqrt{s} = 14$ TeV and 100 fb^{-1} of integrated luminosity.

cut	$WZ \to \ell\ell\ell\nu$	$ZZ \to \ell\ell\ell\ell$	$Zj \to \ell\ell j$	$t\bar{t} \to bb\ell\ell\nu\nu$	signal
basic selection	7240	540	17133	24809	160
$M_T(\ell_1, \not{E}_T) > 120$ GeV	2690	86	1365	11824	132
$\not{E}_T > 100$ GeV	870	20	0	3563	82
$\lvert m_{\ell\ell} - m_Z \rvert < 20$ GeV	380	8	0	355	36
veto on b-jets	379	8	0	272	36
veto on light jet	355	7	0	154	33

TABLE II: The numbers of signal events for $pp \to \chi^0_{1,2}\chi^\pm_1 \to ZG'W^\pm G' \to \ell^+\ell^-\ell^\pm\nu G'G' \to 3\ell + \not{E}_T$ and its statistical significance at the LHC with $\sqrt{s} = 14$ TeV and different luminosities. S_1 and B_1 stand for the signal and background events after basic selection, while S_2 and B_2 stand for the signal and background events after all the cuts.

$\sqrt{s} = 14$ TeV	100 fb^{-1}	500 fb^{-1}	1000 fb^{-1}	1500 fb^{-1}	2000 fb^{-1}	3000 fb^{-1}
$S_{1[\text{basic selection}]}$	160	800	1600	2400	3200	4800
$S_{2[\text{passing all cuts}]}$	33	165	330	495	660	990
$S_1/\sqrt{S_1 + B_1}$	0.7	1.6	2.3	2.8	3.2	3.9
$S_2/\sqrt{S_2 + B_2}$	1.4	3.1	4.5	5.5	6.3	7.7

case. Thus the signal is a single lepton and two bottom quarks with large missing transverse energy:

$$pp \to \chi^0_1\chi^\pm_1 \to hW^\pm G'G' \to \ell^\pm b\bar{b}\nu G'G' \to \ell + 2b + \not{E}_T \quad (\ell = e, \mu, \tau). \tag{21}$$

In the calculation we fix the relevant parameters as $M_2 = 200$ GeV, $\mu = 1.0$ TeV and $M_1 = 1.5$ TeV. The other parameters are assumed to take the same values as in the Higgsino-like case.

The dominant SM backgrounds for this signal are diboson productions, $Wb\bar{b}$, top pair and single top productions. For diboson productions, we only consider the WZ production where Z decays to $b\bar{b}$ and W decays leptonically. The contribution from other diboson productions should be very small. For the $Wb\bar{b}$ production, its contribution may be suppressed by requiring large missing transverse energy. The top pair production can mimic the signal if one of the W bosons decays leptonically. The single top production can also fake the signal when the light quark is misidentified as a b-quark or missing transverse energy.

In Fig. 4 we present the normalized M_T and $\not{E}_T$ distributions of the signal and back-

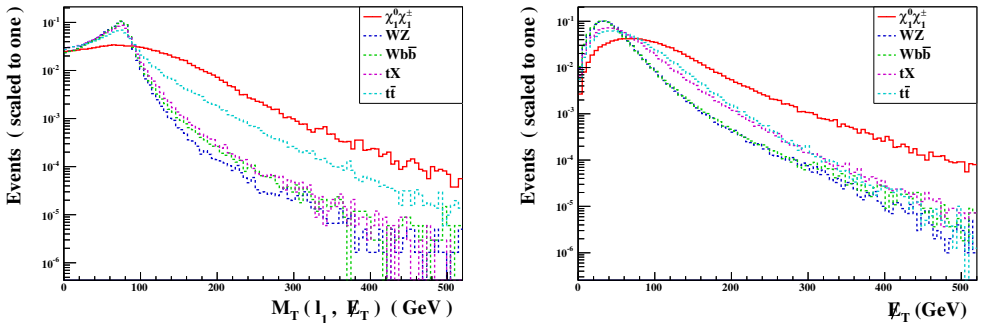

FIG. 4: The normalized M_T and $\not{E}_T$ distributions for the signal $pp \to \chi_1^0\chi_1^\pm \to hW^\pm G'G' \to \ell^\pm \nu b\bar{b}G'G' \to \ell + 2b + \not{E}_T$ and backgrounds at the LHC with $\sqrt{s} = 14$ TeV. For the signal we fixed the relevant mass parameter as $M_2 = 200$ GeV, $\mu = 1.0$ TeV, $M_1 = 1.5$ TeV. The other parameters are same as in Fig. 3.

grounds at the 14 TeV LHC. It is expected that the peak of the transverse mass distribution for the backgrounds with a single W is around m_W. Including di-leptonical channels, the shape of the curves for top pair production should be a little different. We can observe that the transverse mass cut should be effective for suppressing the backgrounds. In the missing transverse energy distribution, we see that the signal has a slightly harder $\not{E}_T$ spectrum due to the contribution of goldstini. Thus a hard cut on $\not{E}_T$ will further reduce the backgrounds. At last we employ the following selections for this signal:

- Basic selection: one isolated lepton with $p_T > 40$ GeV, $|\eta| < 2.5$ and two tagged b-jets with $p_T^{b_1,b_2} > 60, 40$ GeV, $|\eta| < 2.5$.
- The invariant mass of b-jets must be within $|m_{bb} - m_h| < 25$ GeV.
- $M_T > 100$ GeV.
- $\not{E}_T > 120$ GeV.

In Table III we display the cut flow for the signal and backgrounds at the LHC with $\sqrt{s} = 14$ TeV and an integrated luminosity of 100 fb^{-1}. Note that we have normalized the dominant $t\bar{t}$ background to NNLO [32]. We see that the invariant mass cut strongly suppresses the backgrounds, while having little effect on the signal. As we have shown in Fig. 4, the rather hard cuts on M_T and $\not{E}_T$ can efficiently reduce the SM backgrounds. We observe from Table III that these cuts can almost remove the $Wb\bar{b}$ background. The dominant top pair and single top backgrounds are also reduced by about several orders of magnitude. However, the signal is only suppressed by a factor of seven.

TABLE III: The numbers of events for signal $pp \to \chi_1^0\chi_1^\pm \to hW^\pm G'G' \to \ell^\pm b\bar{b}\nu G'G' \to \ell + 2b + \not{E}_T$ and backgrounds for the LHC with $\sqrt{s} = 14$ TeV and 100 fb^{-1} of integrated luminosity.

cut	$WZ \to \ell\nu b\bar{b}$	$Wb\bar{b} \to \ell\nu b\bar{b}$	$tX \to \ell b\nu X$	$t\bar{t} \to b\bar{b}\ell\nu\ell\nu(qq')$	signal
basic selection	373	7845	50015	796066	956
$\|m_{bb} - m_h\| < 25$ GeV	82	1913	13164	199941	769
$M_T > 100$ GeV	4	220	1215	27845	367
$\not{E}_T > 120$ GeV	1	3	69	2617	149

TABLE IV: The number of the signal events $pp \to \chi_1^0\chi_1^\pm \to hW^\pm G'G' \to \ell^\pm b\bar{b}\nu G'G' \to \ell + 2b + \not{E}_T$ and its statistical significance for the LHC with $\sqrt{s} = 14$ TeV and different luminosities. S_1 and B_1 stand for the signal and background events after basic selection, while S_2 and B_2 stand for the signal and background events after all the cuts.

$\sqrt{s} = 14$ TeV	100 fb^{-1}	200 fb^{-1}	300 fb^{-1}	400 fb^{-1}	500 fb^{-1}	600 fb^{-1}
$S_{1[\text{basic selection}]}$	956	1912	2868	3824	4780	5736
$S_{2[\text{passing all cuts}]}$	149	298	447	596	745	894
$S_1/\sqrt{S_1 + B_1}$	1.0	1.5	1.8	2.1	2.3	2.5
$S_2/\sqrt{S_2 + B_2}$	2.8	4.0	4.8	5.6	6.3	6.8

In Table IV we present the number of signal events and its statistical significance for different luminosities at the 14 TeV LHC. As expected, these optimization cuts improved the signal significance efficiently. We see that the significance can reach 5σ for an integrated luminosity of about 300 fb^{-1}. We also notice that the ratio of signal-to-background is only about 6%. This implies that the systematic uncertainty must be controlled at percent level in order to detect the signal in this case.

C. Bino-like LOSP ($M_1 < M_2, |\,\mu\,|$)

In this case the lightest neutralino is bino-like and its pair production cross section is small at the LHC (10^{-6}–10^{-7} pb). For the next lightest ordinary supersymmetric particle (NLOSP), its components depend on the relative values of M_2 and μ. In the following we investigate the different scenarios: (i) $|\mu| < M_2$, in which the next lightest neutrilino χ_2^0 and chargino $\chi_1^\pm$ are higgsino-like; (ii) $M_2 < |\mu|$, in which the next lightest neutrilino χ_2^0 and chargino $\chi_1^\pm$ are wino-like. In both scenarios, the leading production channels are the NLOSP pair production. Since the decay of the neutral NLOSP is more sensitive to the

SUSY parameters than the charged NLOSP, we therefore only explore the charged NLOSP pair ($\chi_1^+\chi_1^-$) production. Here the chargino dominantly decays to a W boson plus a bino-like LOSP χ_1^0 or goldstini G'.

In case of a higgsino-like $\chi_1^\pm$, due to the relative large higgsino-bino mixing, $\chi_1^\pm$ dominantly decays to χ_1^0 and W boson. As discussed in Section II, a bino-like χ_1^0 decays to Higgs and goldstini G'. Then this channel is $pp \to \chi_1^+\chi_1^- \to \chi_1^0 W^+ \chi_1^0 W^- \to hhW^+W^-G'G'$ (6.7 fb). So its cross section is too small to be detected at the LHC.

In case of a wino-like $\chi_1^\pm$, there is little mixing between bino and wino. Then $\chi_1^\pm$ will decay to goldstini G' and W boson. Thus the signal is

$$pp \to \chi_1^+\chi_1^- \to W^+G'W^-G' \to \ell^+\ell^-\nu\nu G'G' \to 2\ell + \not{E}_T \quad (l = e, \mu, \tau). \tag{22}$$

The characteristic of this signal is two highly boosted leptons and large missing transverse energy in the final state. This feature will help to distinguish the signal from backgrounds. In our analysis the bino-like LOSP neutralino is set as $M_1 = 200$ GeV. Also, we set $M_2 = 500$ GeV and $\mu = 1.0$ TeV, and other parameters are the same as in the higgsino-like LOSP case.

The SM backgrounds come from the diboson productions of WW, ZZ and WZ, the top pair and single top productions. The WW background can be suppressed by requiring large missing transverse energy. For ZZ background process, when one of Z bosons decays to leptons and the other to neutrinos, it can resemble our signal. These two leptons are different from the signal with highly boosted leptons. Thus a high invariant mass cut on the two leptons could reduce this background. For the WZ background, it will fake the signal only if one of three leptons in the final state is missing detection. The two W bosons produced in $t\bar{t}$ and tW processes decay to leptons and thus can fake our signal. These processes could be suppressed by applying b-jet and light jet vetos. Since we require large transverse energy, the W/Z production associated with a jet or photon will not be considered in our work.

In Fig. 5 we show the normalized M_T distributions of the hard and light charged leptons for the signal and backgrounds at the 14 TeV LHC. Since both leptons in the signal come from the decays of heavy particles, the signal has harder spectrum than backgrounds in the M_T distributions. We notice that the backgrounds in the $M_T(\ell_2, \not{E}_T)$ distribution have faster falling than in the $M_T(\ell_1, \not{E}_T)$ distribution. Thus we will require a cut on $M_T(\ell_2, \not{E}_T)$ to suppress the backgrounds. The normalized $\not{E}_T$ distribution for the signal and backgrounds is also presented in Fig. 5. We see the $\not{E}_T$ distribution for the signal is much harder than the signal due to extra goldstini contribution to the missing energy. We will apply a large missing transverse energy cut to improve the signal significance. Based on the above analysis, we apply the following selection for this signal:

- Basic selection: two opposite-sign leptons with $P_T^{\ell_1,\ell_2} > 60, 40$ GeV, $|\eta| < 2.5$.

- $M_T(\ell_2, \not{E}_T) > 120$ GeV.
- $\not{E}_T > 120$ GeV.
- $M_{\ell^+\ell^-} > 140$ GeV.
- Veto on tagged b-jets with $P_T > 20$ GeV and $|\eta| < 2.5$.
- Veto events with $P_T(j) > 50$ GeV and $|\eta| < 5.0$.

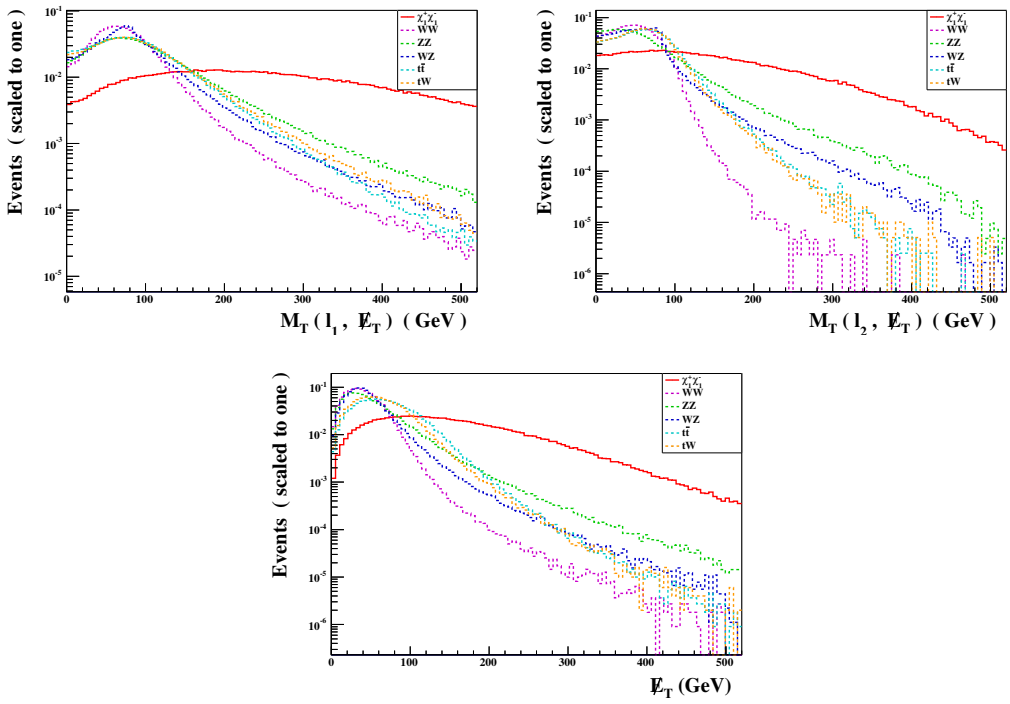

FIG. 5: The normalized M_T and $\not{E}_T$ distribution for the signal $pp \to \chi_1^+\chi_1^- \to W^+G'W^-G' \to \ell^+\ell^-\nu\nu G'G' \to 2\ell + \not{E}_T$ and background processes at the LHC with $\sqrt{s} = 14$ TeV. For the signal we fixed the relevant mass parameters as $M_1 = 200$ GeV, $M_2 = 500$ GeV, $\mu = 1.0$ TeV. Other parameters are same as in Fig. 3.

In Table V we present the cut flow for the signal and background events at the LHC with $\sqrt{s} = 14$ TeV and an integrated luminosity of 100 fb^{-1}. We have nomalized the dominant $t\bar{t}$ background to NNLO [32]. We see that the signal is overwhelmed by the backgrounds at the basic selection level. As we expected, the M_T cut on the light lepton can suppress the backgrounds, while keeping most of the signal. This cut is extremely effective for suppressing the WW background. Then the WW background is further suppressed by a hard cut on $\not{E}_T$. The WZ and ZZ backgrounds with two leptons from Z decay are removed by requiring a large invariant mass of leptons. The dominant reducible backgrounds

TABLE V: The numbers of events for signal $pp \to \chi_1^+\chi_1^- \to W^+G'W^-G' \to \ell^+\ell^-\nu\nu G'G' \to 2\ell + \not{E}_T$ and background at the LHC with $\sqrt{s} = 14$ TeV and 100 fb^{-1} of integrated luminosity.

cut	$WW \to \ell\ell\nu\nu$	$ZZ \to \ell\ell\nu\nu$	$WZ \to \ell\ell\ell\nu$	$t\bar{t} \to b\bar{b}\ell\ell\nu\nu$	$tW \to b\ell\ell\nu\nu$	signal
basic selection	30524	1524	1578	599505	52913	102
$M_T(\ell_2, \not{E}_T) > 120$ GeV	744	900	407	84647	6018	65.7
$\not{E}_T > 120$ GeV	12.6	582	180	14381	901	55.5
$M_{\ell^+\ell^-} > 140$ GeV	11.4	0.4	5.3	9759	643	43.3
veto on b-jets	11.1	0.4	5.3	4107	334	43.1
veto on light jet	6.1	0.3	1.9	124	17.9	37.3

TABLE VI: The number of events for the signal $pp \to \chi_1^+\chi_1^- \to W^+G'W^-G' \to \ell^+\ell^-\nu\nu G'G' \to 2\ell + \not{E}_T$ and its statistical significance for the LHC with $\sqrt{s} = 14$ TeV and different luminosities. S_1 and B_1 stand for the signal and background events after basic selection, while S_2 and B_2 stand for the signal and background events after all the cuts.

$\sqrt{s} = 14$ TeV	100 fb^{-1}	200 fb^{-1}	300 fb^{-1}	400 fb^{-1}	500 fb^{-1}	600 fb^{-1}
$S_{1[\text{basic selection}]}$	102	204	306	408	510	612
$S_{2[\text{passing all cuts}]}$	37.3	74.6	112	149	187	224
$S_1/\sqrt{S_1 + B_1}$	0.12	0.17	0.21	0.25	0.28	0.30
$S_2/\sqrt{S_2 + B_2}$	2.7	3.9	4.7	5.4	6.1	6.8

$t\bar{t}$ and tW are suppressed strongly by the veto on b-jets and light jets. After all cuts, the signal-to-background ratio is about 25%.

In Table VI we display the number of signal events and its significance before and after the cuts for different luminosities at the 14 TeV LHC. We see that the significance is improved by these cuts efficiently. The significance can reach 5σ for a luminosity of 300–400 fb^{-1}.

IV. CONCLUSIONS

Goldstini is predicted in the multi-sector SUSY breaking scenario. Comparing to the ordinary gravitino, it can couple to the visible sector more strongly and hence lead to some intriguing phenomenology at colliders. In this scenario the lightest neutralino (chargino) can decay into a goldstini plus a Z-boson or Higgs boson (W-boson). In this work we performed a Monte Carlo simulation for the direct productions of the lightest neutralino and chargino followed by the decays to goldstini. Considering a higgsino-like, bino-like or

wino-like lightest neutralino, we found that the signal-to-background ratio (S/B) is 6%–25% and the statistical significance $S/\sqrt{S+B}$ is 5σ at the high luminosity LHC. So it is feasible to explore such a multi-sector SUSY breaking scenario at the high luminosity LHC if the background is known to percent level.

Acknowledgments

Lin Wang acknowledges Prof. Johann H. Kühn and Prof. Matthias Steinhauser for their warm hospitality. This work is supported by by the Grant-in-Aid for Scientific Research (No. 24540246) from Ministry of Education, Culture, Sports, Science and Technology (MEXT) of Japan, by DFG through SFB/TR 9 "Computational Particle Physics" and by the National Natural Science Foundation of China under grant Nos. 11275245, 10821504 and 11135003.

---

[1] For the status of low energy SUSY models confronted with the LHC Higgs data, see, e.g., M. Carena *et al.* JHEP 1203, 014 (2012); JHEP **1207**, 175 (2012); J. Cao *et al.*, JHEP **1203**, 086 (2012); JHEP **1210**, 079 (2012); Phys. Lett. B **710**, 665 (2012); U. Ellwanger, JHEP 1203, 044 (2012); U. Ellwanger, C. Hugonie, arXiv:1203.5048.

[2] C. Cheung, Y. Nomura, and J. Thaler, JHEP **1003** (2010) 073 [arXiv:1002.1967 [hep-ph]].

[3] C. Cheung, J. Mardon, Y. Nomura, and J. Thaler, JHEP **1007** (2010) 035 [arXiv:1004.4637 [hep-ph]].

[4] K. Benakli and C. Moura, Nucl. Phys. B **791** (2008) 125 [arXiv:0706.3127 [hep-th]].

[5] N. Craig, J. March-Russell, and M. McCullough, JHEP **1010** (2010) 095 [arXiv:1007.1239 [hep-ph]].

[6] M. McCullough, Phys. Rev. D **82** (2010) 115016 [arXiv:1010.3203 [hep-ph]].

[7] K. I. Izawa, Y. Nakai, and T. Shimomura, JHEP **1103** (2011) 007 [arXiv:1101.4633 [hep-ph]].

[8] J. Thaler and Z. Thomas, JHEP **1107** (2011) 060. [arXiv:1103.1631 [hep-ph]].

[9] C. Cheung, F. D'Eramo, and J. Thaler, JHEP **1108** (2011) 115 [arXiv:1104.2600 [hep-ph]].

[10] D. Bertolini, K. Rehermann, and J. Thaler, [arXiv:1111.0628 [hep-ph]].

[11] H. -C. Cheng, W. -C. Huang, I. Low, and A. Menon, JHEP **1103** (2011) 019 [arXiv:1012.5300 [hep-ph]].

[12] K. Mawatari and Y. Takaesu, Eur. Phys. J. C **71**, 1640 (2011).

[13] R. Argurio, Z. Komargodski, and A. Mariotti, Phys. Rev. Lett. **107** (2011) 061601. [arXiv:1102.2386 [hep-th]].

[14] R. Argurio, K. De Causmaecker, G. Ferretti, A. Mariotti, K. Mawatari, and Y. Takaesu, JHEP **1206** (2012) 096 [arXiv:1112.5058 [hep-ph]].

[15] G. Ferretti, A. Mariotti, K. Mawatari, and C. Petersson, arXiv:1312.1698 [hep-ph].

[16] T. Liu, L. Wang, and J. M. Yang, Phys. Lett. B **726** (2013) 228 [arXiv:1301.5479 [hep-ph]].

[17] T. Han, S. Padhi, and S. Su, arXiv:1309.5966 [hep-ph].

[18] S. Samuel and J. Wess, Nucl. Phys. B **221** (1983) 153. R. Casalbuoni, S. De Curtis, D. Dominici, F. Feruglio, and R. Gatto, Phys. Lett. B **220** (1989) 569. Z. Komargodski and N. Seiberg, JHEP **0909** (2009) 066 [arXiv:0907.2441 [hep-th]].

[19] B. C. Allanach, Comput. Phys. Commun. **143** (2002) 305 [hep-ph/0104145].

[20] J. Alwall *et al.*, JHEP **1106**, 128 (2011).

[21] A. Alloul, *et al.*, arXiv:1310.1921 [hep-ph].

[22] C. Degrande, *et al.*, Comput. Phys. Commun. **183** (2012) 1201 [arXiv:1108.2040 [hep-ph]].

[23] T. Sjostrand, L. Lonnblad, S. Mrenna, and P. Z. Skands, hep-ph/0308153.

[24] W. Beenakker *et al.*, Phys. Rev. Lett. **83** (1999) 3780 [Erratum-ibid. **100** (2008) 029901] [hep-ph/9906298].

[25] J. de Favereau *et al.* [DELPHES 3 Collaboration], JHEP **1402** (2014) 057 [arXiv:1307.6346 [hep-ex]].

[26] M. Cacciari, G. P. Salam, and G. Soyez, JHEP **0804**, 063 (2008)

[27] M. Cacciari, G. P. Salam, and G. Soyez, Eur. Phys. J. C **72** (2012) 1896 [arXiv:1111.6097 [hep-ph]].

[28] E. Conte, B. Fuks, and G. Serret, Comput. Phys. Commun. **184** (2013) 222 [arXiv:1206.1599 [hep-ph]].

[29] C. Han *et al.*, arXiv:1310.4274 [hep-ph]; H. Baer, A. Mustafayev and X. Tata, arXiv:1401.1162 [hep-ph].

[30] The ATLAS parametric approach at default in Delphes.

[31] J. M. Campbell, R. K. Ellis, and C. Williams, JHEP **1107** (2011) 018 [arXiv:1105.0020 [hep-ph]].

[32] M. Czakon, P. Fiedler, and A. Mitov, Phys. Rev. Lett. **110** (2013) 252004 [arXiv:1303.6254 [hep-ph]].

[33] S. P. Martin and P. Ramond, Phys. Rev. D **48** (1993) 5365 [hep-ph/9306314].